IEEE Access
Multidisciplinary | Rapid Review | Open Access Journal

Received April 26, 2019, accepted May 19, 2019, date of publication May 23, 2019, date of current version June 5, 2019.

Digital Object Identifier 10.1109/ACCESS.2019.2918504

Fault-Tolerant Operation of Wound Field Synchronous Machine Using Coil Switching

MUHAMMAD AYUB[1], SHAHID ATIQ[2], GHULAM JAWAD SIREWAL[1], AND BYUNG-IL KWON[1], (Senior Member, IEEE)

[1]Department of Electrical and Electronic Engineering, Hanyang University, Ansan 15588, South Korea
[2]Department of Electrical Engineering, Khwaja Fareed University of Engineering and Information Technology, Rahim Yar Khan 64200, Pakistan

Corresponding author: Byung-il Kwon (bikwon@hanyang.ac.kr)

This work was supported in part by the Korea Institute of Energy Technology Evaluation and Planning (KETEP), in part by the Ministry of Trade, Industry and Energy (MOTIE), South Korea, under Grant 20174030201780, and in part by the National Research Foundation of Korea through the BK21PLUS Program within the Ministry of Education.

ABSTRACT This paper proposes a fault tolerant operation of a wound field synchronous machine (WFSM) under the loss of excitation (LOE) fault in the rotor field winding. A two-mode field excitation scheme is presented, where the rotor of the WFSM was modified, and an additional harmonic winding is introduced with a rotating bridge rectifier. Mode I is the conventional direct dc supply field excitation using slip-rings and brushes, whereas mode II, is the brushless field excitation under an LOE fault, resulting in an unregulated field current. During mode II, a special coil switching is performed in the stator. Consequently, the stator winding creates an additional sub-harmonic component of the magneto-motive force (MMF) in the machine air gap along with the fundamental MMF component. The additional sub-harmonic MMF is induced in the rotor harmonic winding. A rotating diode bridge rectifier mounted on the rotor periphery rectifies the harmonic winding ac, and a stable dc was supplied to the rotor field winding. The decoupling between the additional rotor harmonic winding and stator winding is analyzed. The 2-D finite-element analysis (FEA) was performed to analyze the proposed idea. The FEA results were validated by experiments based on a 1-kW prototype.

INDEX TERMS Brushless excitation, coil switching, fault-tolerant operation, wound field synchronous machine.

I. INTRODUCTION

Wound field synchronous machines (WFSMs) [1]–[5] have a serious problem with respect to the rotor excitation mechanism. The brushes, slip-rings or exciter start to malfunction during extended operation as shown in Fig. 1. Malfunctioning of any of the excitation components halts machine operation. The resulting loss of excitation (LOE) or loss of connectivity of DC supply to the rotor field winding can be a disaster with violent vibrations and rotor heating. To prevent the potential loss of system and equipment, and fault travel to the connected grid, protection relays are used to detect the excitation loss and bring the machine to a stop autonomously [6]–[7]. However, in small and medium synchronous machine applications where stand-alone operation is required, there is a potential loss of productivity associated with the repair of the fault. During the repair time, the machine is unable to generate an output since the rotor field is not present on the rotor. It is even worse when relay protection sends signal to the trip circuit in false alarm conditions. The problem is

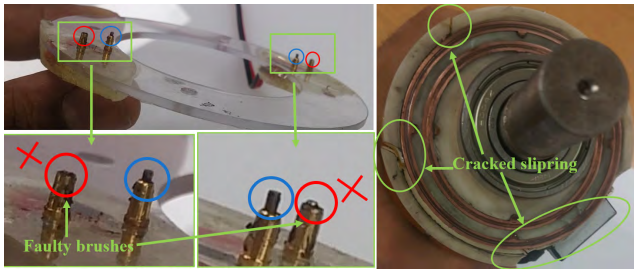

FIGURE 1. Faulty brushes and slipring.

The associate editor coordinating the review of this manuscript and approving it for publication was Shen Yin.

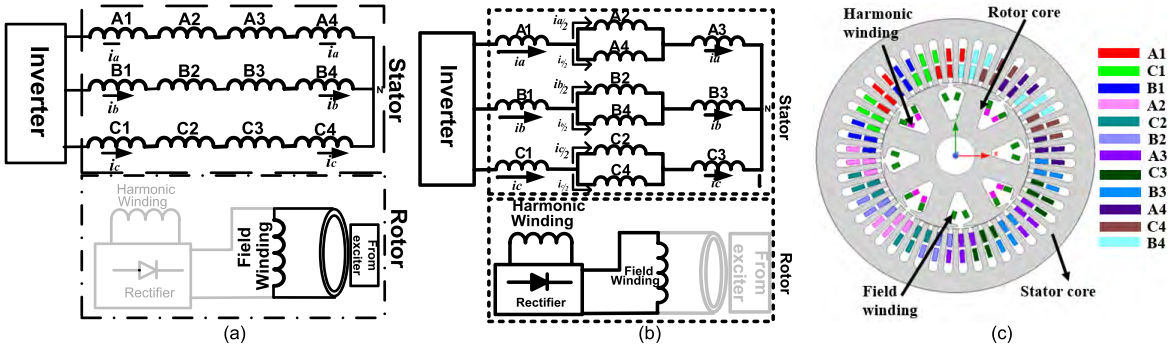

FIGURE 2. Two mode of operations (a) Mode I, (b) Mode II, and (c) Machine layout.

conventionally dealt with by providing redundant protection and the choice of relay or protection system is crucial in this regard as discussed in [6]. Moreover, the incorporation of power flow controllers and other machine protection equipment may cause delay or false operation of the LOE relay to generate a trip signal [8]. To address this problem, the faulty machine could be utilized based on a brushless harmonic excitation technique, where the field is induced in the rotor field winding by utilizing an additional stator harmonic magneto-motive force (MMF). There are several brushless topologies available in the literature that mainly focus on brushless operation of the WFSM [9]–[17]. Brushless operation of the WFSM has been achieved by generating an extra MMF component alongside the fundamental MMF component.

Concerning brushless operation, in [10], a self-excited three-phase brushless synchronous machine was analyzed, in which the 5th harmonic of the MMF was utilized for a generator application. The winding arrangement and control were very simple due to the elimination of the excitation winding of the stator, which resulted in a more robust and cost-effective arrangement.

In [11] a single inverter is used to supply three-phase sinusoidal currents and consecutive switching of six extra thyristors with natural commutation create zero sequence third harmonic currents resulting in generation of a 3rd harmonic air-gap MMF. Similarly, a 3rd harmonic current excited machine was proposed in [12], [13] where MMF was generated by injecting 3rd harmonic currents in the open pattern armature windings for rotor excitation which removes the need for brushes and slip rings. However, the brushless schemes which utilize time harmonics for rotor excitation adopt complicated control for brushless operation.

In [14]–[18], the field winding was excited by utilizing the spatially generated sub-harmonic MMF component in the machine air gap. In [14], [15], two inverters were used to supply different current magnitudes to two separate stator windings (ABC and XYZ winding). This arrangement produced a sub-harmonic MMF component in the air gap, which was intercepted by the same number of poles of rotor harmonic winding. Since two inverters were utilized in this brushless topology, the practicality was low given the low power density and high cost of the system for a small-medium stand-alone energy conversion application.

In [16]–[19] a single inverter with special stator winding was used for brushless operation. In [20], a WFSM is analyzed for dual stator and dual mode operation for wide speed range operation. Nevertheless, mode changing operation was used in the machine for mainly brushless operation above base speed. The state-of-the-art literature used brushless topologies to avoid the brushes and slip rings available with the conventional WFSM at the cost of low power densities. However, brushless excitation has never been analyzed to avoid LOE fault in the WFSM.

In this paper, a fault tolerant operation of a WFSM under fault of LOE is proposed, where two modes of operation are performed. To operate the machine in two modes, the rotor of a conventional WFSM is modified and an additional harmonic winding is introduced with a rotatable bridge rectifier. Mode I is a conventional WFSM. Whereas, in mode II, the WFSM is operated when the machine is under LOE fault condition. In mode II, a coil switching operation is performed at the stator winding by detecting a field current lower than the reference value using conventional LOE relay. The relay operation signal is fed to the mode changing mechanism instead of a trip breaker. 2D finite-element analysis (FEA) is performed to predict the operation of the machine in both modes. In the end, experiments are performed to validate the FEA predictions.

II. MACHINE TOPOLOGIES WITH WORKING PRINCIPLE

A. MACHINE TOPOLOGIES

The topologies for conventional WFSM (mode I) and fault tolerant (mode II) are given in Fig. 2(a) and 2(b), respectively. The WFSM topologies have a three-phase inverter to feed current into each phase consisting of four coils, i.e., 1-4, with the same number of turns. The rotor of the WFSM has an additional harmonic winding and a field winding which is interconnected through a rotatable bridge rectifier. In mode I, the field is excited by a dc supplied by an external exciter through brushes and slip rings. The dc current is fed from a power supply with voltage less than the diode break-down

TABLE 1. Machine design parameters.

Unit	Parameters	value
kW	Rated power	1
rpm	Rated speed	900
Arms	Rated current	5
mm	Stator outer diameter	177
mm	Stator inner diameter	95
mm	Airgap length	0.5
mm	Stack length	80
-	Pole / slot	8 / 48
-	Stator turns per phase	320
-	Field winding turns	200
-	Harmonic winding turns	48

voltage value. In mode II (as explained in section III), coil switching operation is performed and coils 2 and 4 in each phase are reconnected as parallel to each other to form an arrangement as shown in Fig. 2 (b). This stator winding arrangement is adopted to generate a sub-harmonic MMF component in the air gap for brushless field excitation.

B. WORKING PRINCIPLE

A 48-slot and 8-pole WFSM layout is shown in Fig. 2(c), and the machine parameters are given in Table 1. In the case of mode I, a balanced current is supplied by a three-phase inverter to the topology shown in Fig. 2(a). The stator winding coils in each phase are connected in series. The machine airgap MMF in mode I, ignoring higher harmonics, is given as:

$$F(\theta, t) = \frac{4}{\pi} F_m \sin(\omega t - \theta) \tag{1}$$

The predicted machine airgap MMF (mode I) for the t = 0 is shown in Fig. 3. Since machine operates as a conventional WFSM in mode I, a balanced airgap MMF is predicted with a frequency equivalent to that of the supply currents.

When a fault occurs in any of the excitation components a LOE signal is generated and a coil switching is performed that arranges the machine topology in Fig. 2(a) (mode I) to the machine topology given in Fig. 2(b) (mode II). The coil switching operation is explained in next section. The machine topology in mode II as given in Fig. 2(b) produces a sub-harmonic MMF component alongside the fundamental MMF in the machine air gap [9]. The predicted MMF is given as:

$$\begin{aligned} F(\theta, t) &= \frac{3}{\pi} F_m \sin(\omega t - \theta) \\ &+ \frac{1}{\pi} F_m \left[\begin{array}{l} \sin(\frac{\omega t}{2}) \cos(\theta) + \sin(\frac{\omega t - \frac{2\pi}{3}}{2}) \cos(\theta - \frac{2\pi}{3}) + \\ \sin(\frac{\omega t + \frac{2\pi}{3}}{2}) \cos(\theta + \frac{2\pi}{3}) \end{array} \right] \end{aligned} \tag{2}$$

After simplifying (2), we have:

$$F(\theta, t) = \frac{3}{\pi} F_m \sin(\omega t - \theta) + \frac{1}{\pi} F_m \cos(\frac{\omega t - \theta}{2}) \tag{3}$$

where the second term in (3) represents the sub-harmonic MMF component. All higher harmonics are ignored in (1), (2) and (3).

The estimated airgap MMF at t = 0 in mode II is shown in Fig. 3. The MMF pattern shows that from $0 \rightarrow \pi/2$ and $\pi \rightarrow 3\pi/2$ radians, rated peaks of MMF were generated. The stator currents, as well as the winding function, are at rated values. Similarly, from $\pi/2 \rightarrow \pi$ and $3\pi/2 \rightarrow 2\pi$ radians, the winding coil groups produces half of the rated MMF because the stator current is divided by 2 according to Kirchhoff's current law. The machine airgap MMF shape has a significant amount of sub-harmonic MMF alongside the fundamental MMF component. The sub-harmonic MMF induces in the rotor harmonic winding and the rectified dc current produces the rotor field flux.

III. COIL SWITCHING MECHANISM DESIGN AND OPERATION

The stator winding is wound for an 8-pole arrangement. Each phase is divided into 4 coils, i.e., B_1, B_2, B_3 and B_4 for phase B. The block diagram of the coil switching process with vector controlled WFSM is shown in Fig. 4. The stator winding of the WFSM and the vector-controlled inverter are connected to the switches. There are three switches for each phase to facilitate mode change operation. The switching pattern is given in Table 2, which shows the arrangement of the switches for each phase with both modes. It is shown that for mode I operation, the switch S1 is ON, whereas S2 and S3 are in the OFF states. After the occurrence of a fault in any part of the excitation system, the LOE relay generates a coil switching signal, where, one signal is sent to the PWM

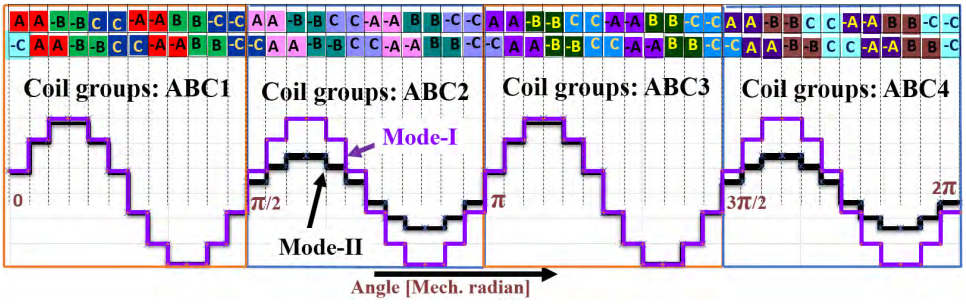

FIGURE 3. Machine airgap MMF for mode I and mode II at t = 0.

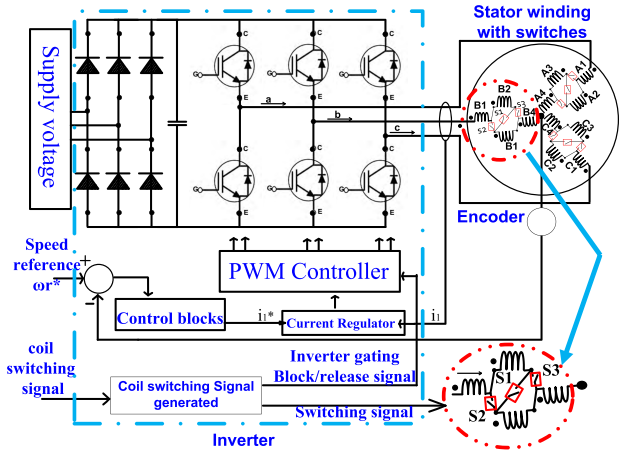

FIGURE 4. Block diagram of coil switching process.

TABLE 2. Coil switching pattern for both modes.

Phase	Switch	Mode I	Mode II
A	S1	ON	OFF
	S2	OFF	ON
	S3	OFF	ON
B	S1	ON	OFF
	S2	OFF	ON
	S3	OFF	ON
C	S1	ON	OFF
	S2	OFF	ON
	S3	OFF	ON

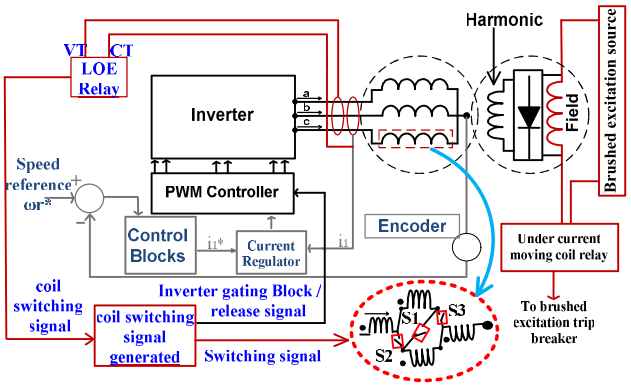

FIGURE 5. Coil switching strategy.

controller to halt the output current. The second signal is then sent to the stator coil switches (S1, S2, and S3) to perform the coil switching, as given in Table 2.

The proposed coil switching strategy stops the inverter current and voltage during mode change. Therefore, transients in current and voltage are neglected in this paper.

The coil switching operation is performed as described below:

Algorithm for coil switching of WFSM under fault (Fig. 5)

1. Obtain the rotor excitation system fault information from LOE relay
2. The coil switching signal is generated
3. Inverter gating block signal is transmitted to PWM controller
4. Wait (for 5 time period)
5. Switching signal is transmitted to coils switches
6. Wait (for 5 time period)
7. Inverter gating release signal is transmitted to PWM controller

Fig. 5 shows the changing mechanism of brushed excitation to brushless by using LOE relay and the ''under current moving coil relay''. The LOE relay input signals are obtained from current transformer (CT) and voltage transformer (VT) on the stator armature windings [8]. The output signal from the LOE relay is sent to coil switching generator for coils switching from series to parallel by the three switches as shown in Fig. 5. Meanwhile the under current relay disconnects the brushed excitation source and the induced voltage in the harmonic winding is rectified and fed to the field winding for harmonic excitation.

To avoid the sudden change in the switch state which could cause an undesirable surge in the current and voltage, a relatively simple method is adopted where the inverter is momentarily suspended during coil switching. Once the desired coil switching is performed the inverter is reenabled.

IV. DECOUPLING ANALYSIS BETWEEN THE ROTOR HARMONIC WINDING AND STATOR WINDING

Since there is an extra 4-pole winding on the rotor, the harmonic winding, therefore, to check the magnetic decoupling between the 4-pole rotor harmonic winding and 8-pole stator winding and vice versa, the following analysis is performed. To verify the decoupling between the two windings [19], [21]–[23], a fictitious 8-pole stator (only phase-A) and 4-pole rotor harmonic winding has been considered and shown in Fig. 6. The electromagnetic decoupling of the two windings having 4-poles and 8-poles are derived in this section.

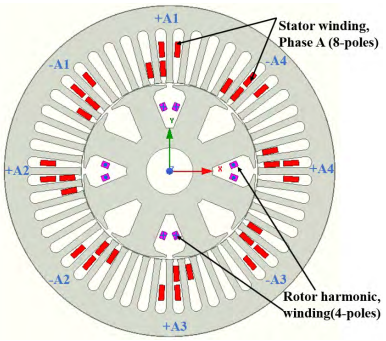

FIGURE 6. Decoupling analysis (fictitious model).

In Fig. 6, the stator coil pitch is 45° degrees (8-poles), while the rotor harmonic coil pitch is 90° degrees (4-poles). When the 4-pole harmonic flux is imposed on the 8-pole armature winding, the armature winding seems short-pitched by 180° degrees. Hence the flux linkages of stator coils of phase-A

due to rotor harmonic flux are given by

$$\begin{aligned}
\lambda_{A_1,-A_1} &= k_w N_{coilA1}\phi_h \cos\left(\frac{\pi}{2}\right)\cos\left(2\theta_m\right)\\
\lambda_{A_2,-A_2} &= k_w N_{coilA2}\phi_h \cos\left(\frac{\pi}{2}\right)\cos\left(2(\theta_m-\frac{\pi}{2})\right)\\
\lambda_{A_3,-A_3} &= k_w N_{coilA3}\phi_h \cos\left(\frac{\pi}{2}\right)\cos\left(2(\theta_m-\pi)\right)\\
\lambda_{A_4,-A_4} &= k_w N_{coilA4}\phi_h \cos\left(\frac{\pi}{2}\right)\cos\left(2(\theta_m-\frac{3\pi}{2})\right)
\end{aligned} \tag{4}$$

where, $\lambda_{A,-A}$ are the flux linkages on the stator each coil due to rotor harmonic flux, k_w is the winding factor, N_{coilA} number of turns of each coil with in phase A, ϕ_h is the rotor harmonic flux.

From (4), the induced EMFs in each stator coil is calculated as

$$\begin{aligned}
e_{A_1,-A_1} &= -2\omega_m k_w N_{coilA1}\phi_h \cos\left(\frac{\pi}{2}\right)\sin\left(2\omega_m t\right)\\
e_{A_2,-A_2} &= -2\omega_m k_w N_{coilA2}\phi_h \cos\left(\frac{\pi}{2}\right)\sin\left(2(\omega_m t-\frac{\pi}{2})\right)\\
e_{A_3,-A_3} &= -2\omega_m k_w N_{coilA3}\phi_h \cos\left(\frac{\pi}{2}\right)\sin\left(2(\omega_m t-\pi)\right)\\
e_{A_4,-A_4} &= -2\omega_m k_w N_{coilA4}\phi_h \cos\left(\frac{\pi}{2}\right)\sin\left(2(\omega_m t-\frac{3\pi}{2})\right)
\end{aligned} \tag{5}$$

where, $\theta_m = \omega_m t$, and ω_m is the angular speed.

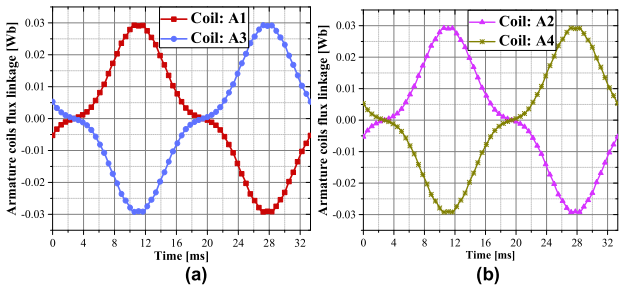

FIGURE 7. Stator coils flux linkage due to rotor harmonic winding flux (a) stator coils A1 and A3 and (b) stator coils A2 and A4.

Therefore, the total induced EMF in the coils of phase-A is

$$e_{A_1,-A_1} + e_{A_2,-A_2} + e_{A_3,-A_3} + e_{A_4,-A_4} = 0 \tag{6}$$

Equation (6) shows there is no mutual coupling between the rotor harmonic winding (4-pole) and stator winding (8-pole). To verify the decoupling the FEA is performed. A 5 A dc current is applied to the rotor harmonic winding, whereas, stator winding coils are kept open. The flux linkage on the stator individual coils (phase-A) is shown in Fig. 7, where Fig. 7(a) shows the flux linkages of phase-A coils: 1 and 3, and Fig. 7(b) shows the flux linkages of phase-A coils: 2 and 4. The Fig. 8 shows the net flux linkage due to all four coils, since each pair of coils (1, 3 and 2, 4) has the flux linkage which is out of phase by 180° degrees therefore the net flux linkage is almost zero. The induced voltage in the coils of phase-A is shown in Fig. 9, where Fig. 9(a) shows

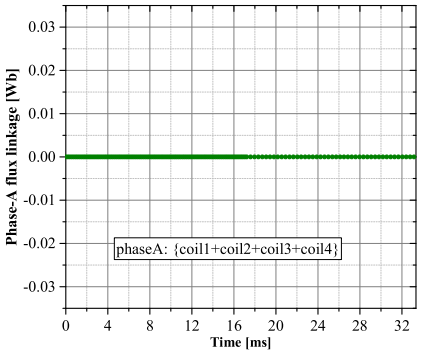

FIGURE 8. Phase-A flux linkage due to rotor harmonic winding flux.

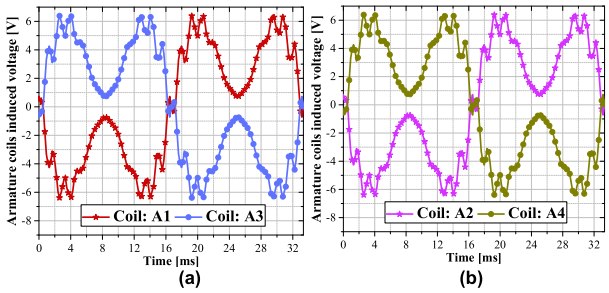

FIGURE 9. Stator coils induced voltages due to rotor harmonic winding flux (a) stator coils A1 and A3 (b) stator coils A2 and A4.

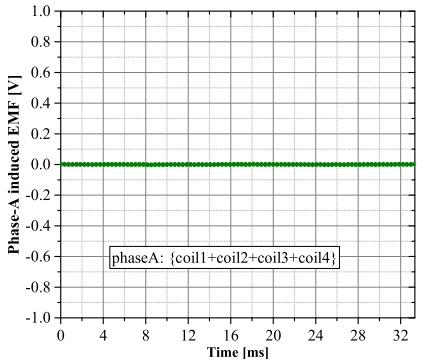

FIGURE 10. Phase-A induced voltage due to rotor harmonic winding flux.

the induced EMF of phase-A coils: 1 and 3, and Fig. 9(b) shows the induced EMF of phase-A coils: 2 and 4. The induced EMF in phase-A is shown in Fig. 10. It is shown that due to 180° degrees out of phase in phase individual induced EMF the net induced EMF is almost zero. Thus, the simulation results verified that the 4-pole rotor harmonic winding and 8-pole stator winding is mutually decoupled, and do not contribute interference for each other.

V. PERFORMANCE ANALYSIS OF THE MACHINE USING FEA

A 2-D FEA was performed to verify the proposed fault tolerant operation of the WFSM. An 8-pole and 48-slot machine was considered with the parameters given in Table 1.

Initially, the machine is analyzed for no-load back-EMF in mode I, where switch S1 is ON, and S2 and S3 are OFF.

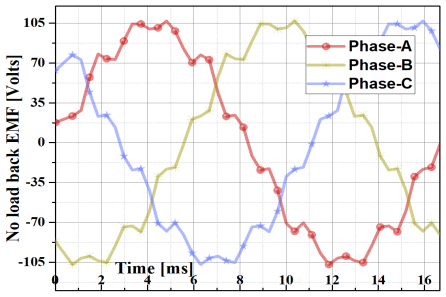

FIGURE 11. No-load back EMF (FEA).

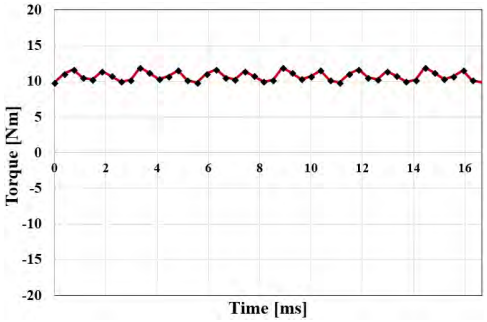

FIGURE 12. Mode I: electromagnetic torque (FEA).

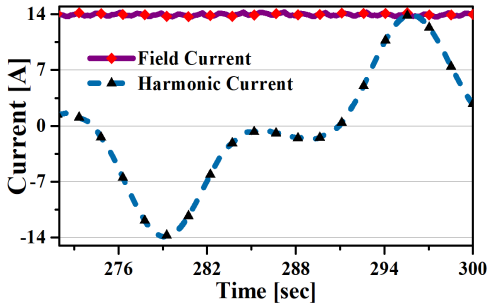

FIGURE 13. Mode II: rotor currents (FEA).

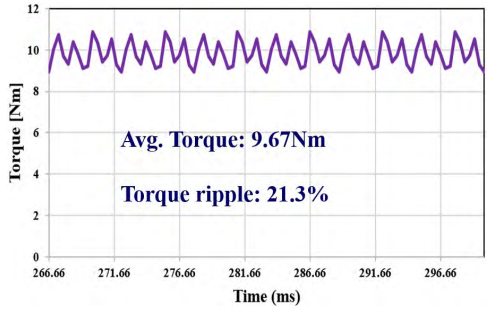

FIGURE 14. Mode II: electromagnetic torque (FEA).

The stator winding coils are connected in series in this mode. A 10 A dc field current is applied through machine brushes and slip rings. The rotor is rotated at 900 rpm. The three-phase balance back-EMF is shown in Fig. 11 with a rms value of 72.80 V for each phase. Once the balanced no-load back-EMF is achieved, the stator of the machine is supplied with a balanced three-phase 5 A rms current in-phase with the back-EMF. The electromagnetic torque is shown in Fig. 12. In the case of mode I, since the field winding of the machine is supplied via the external exciter, the rotor harmonic winding does not have any current. The field current is blocked towards the harmonic winding by the reverse bias diodes present in the rotating bridge rectifier.

The machine is analyzed in mode II by changing the stator winding as given in Fig. 2(b). In this mode, the machine operated as a brushless WFSM. The balanced three-phase 5 A rms current at 60 Hz is applied to the stator winding of the machine. The winding arrangement was able to generate a sub-harmonic MMF component in the machine airgap alongside the fundamental MMF. The sub-harmonic MMF was induced in the same pole pitch rotor harmonic winding. The rotating rectifier rectified the harmonic winding current and a steady state dc current was applied to the rotor field winding. Fig. 13 shows the rotor harmonic and field winding currents, where, a 4.6 A rms current is induced in the rotor harmonic winding. After rectification, the rotor field winding was able to establish a 14 A dc current.

The flux density given in Fig. 15 clearly shows that the machine core is well below the maximum flux density of 2 tesla (T). Similarly, the flux line distributions in the machine core show the flux pattern in both the modes of the proposed topology. The flux density and flux line distribution pattern clearly show the different mode of operation. As explained in the section III, the modes of the machine were changed by a coil switching strategy. The air gap flux density distributions are also shown in Fig. 15 of both the modes for proposed WFSM topology. Since we know that the mode I is a brushed synchronous machine, therefore the air gap flux density distribution shows symmetrical 4-pole pairs. On the other side, in mode II, since the coils are switched for a fault tolerant operation, therefore, asymmetrical air gap flux density distribution could be observed. The asymmetrical air gap flux density distribution shows additional low frequency harmonic flux component. To check the frequency spectrum of the air gap flux density distribution, we have applied fast Fourier transform (FFT) in 2-D FEM software. The FFT result given in Fig. 15 gave us the harmonic spectra of the flux density. In mode I, the FFT analysis shows that there is a fundamental 4-pole pair component and higher order 12- and 20-pole pairs. In mode II, the FFT analysis shows that alongside 4-pole pairs fundamental flux component there is a 2-pole pairs sub-harmonic component. The 2-pole pair sub-harmonic is induced in the rotor harmonic winding and then used for field excitation in mode II. After excitation of the rotor field poles; the field flux interacted with the fundamental harmonic MMF and electromagnetic torque is generated.

The electromagnetic torque in mode I was 10.76 Nm with a torque ripple of 19.3%, as shown in Fig. 12, whereas the electromagnetic torque in mode II was 9.67 Nm with a torque ripple of 21.2%, as shown in Fig. 14. The decrease of the torque in mode II from mode I is due to the absence of

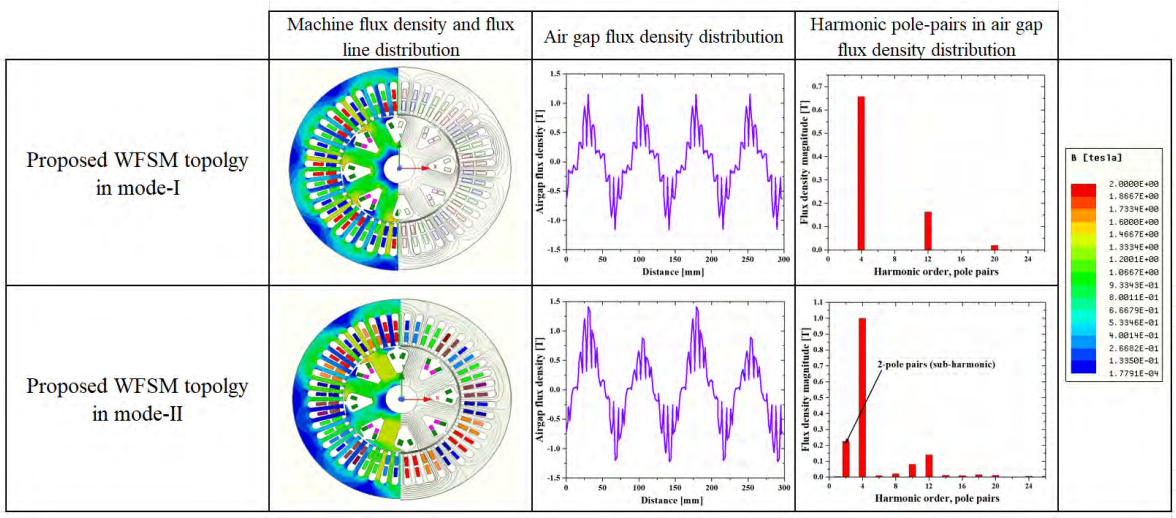

FIGURE 15. 2-D FEA analysis of the proposed WFSM topology in mode I and mode II.

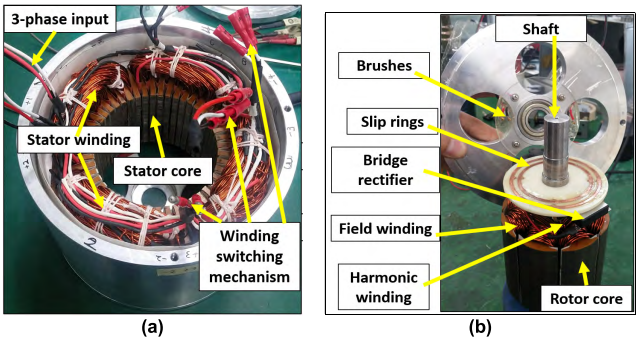

FIGURE 16. Manufactured prototype (a) stator and (b) rotor.

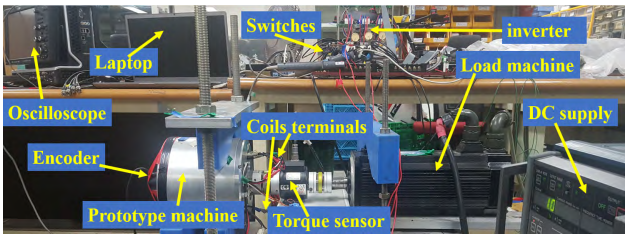

FIGURE 17. Experimental setup.

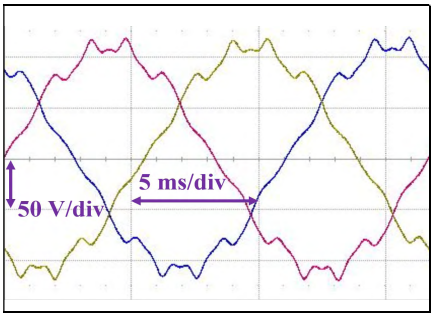

FIGURE 18. No-load back EMF (experiment).

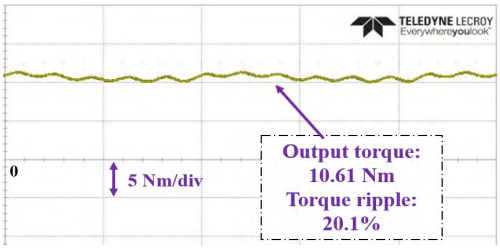

FIGURE 19. Mode I: output torque (experiment).

the rotor dc field current. In mode II, the rotor field current is established based on the stator input current. The torque ripple shows a 3.04% increase in mode II. This increase is mainly due to the generation of unwanted components in the flux apart from sub-harmonic and fundamental harmonic component.

VI. EXPERIMENTAL VERIFICATION

The FEA predictions highlighted in section V have been verified by experiments on a 1 kW prototype. The prototype was designed with the parameters given in Table 1. The prototype rotor and stator with coil switching terminals are shown in Fig. 16. The Fig. 17 shows the experimental setup.

To verify the no-load back-EMF, the rotor field winding was supplied with a 10 A dc current. A prime mover (induction motor) was coupled to the prototype and was rotated at the rated speed of 900 rpm. A balanced three-phase back-EMF was induced in the prototype machine stator winding. The induced back-EMF is shown in Fig. 18, where a rms value of 71.35 V is observed for each phase.

To operate the prototype as a conventional WFSM, a 5 A rms rated current was supplied to the stator winding and a 10 A dc current was supplied to the rotor field winding. The mode I output torque is given in Fig. 19. The machine was able to produce 10.61 Nm of torque with a torque ripple of 20.1% at the rated speed of 900 rpm.

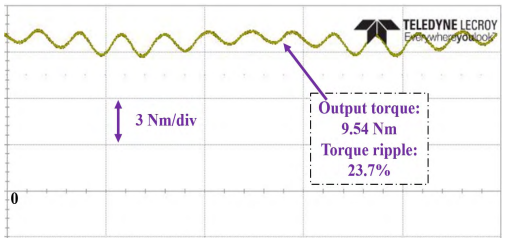

FIGURE 20. Mode II: output torque (experiment).

TABLE 3. Comparison of FEA and experiment analysis.

Units	Quantity	Modes	FEA	Experiment
V rms	Back-EMF	Mode I	72.80	71.35
Nm	Torque (brushed)	Mode I	10.76	10.61
%	Torque ripple	Mode I	19.3	20.1
Nm	Torque (brushless)	Mode II	9.67	9.54
%	Torque ripple	Mode II	21.2	23.7

Considering a fictitious fault created in the rotor dc field current, coil switching was performed as explained. The inverter current was temporarily turned off by the coil switching control signal. Once the coil switching was performed, the inverter was turned on again. The generated sub-harmonic MMF, as explained in the previous sections, was collected by the rotor harmonic winding and after rectification, a dc current was established in the rotor field winding. Since we did not have any mechanism to observe the rotor harmonic and field currents during the shaft rotation in mode II, therefore, the harmonic induction was verified by the shaft torque. The output torque is shown in Fig. 20. It is shown that a 9.54 Nm torque with a 23.7% torque ripple is achieved at a rated speed of 900 rpm. Since the inverter currents, during coil switching process, were temporary suspended therefore transients were not created in the phase currents and voltages during the mode change. A comparison between the FEA and experimental results for both modes is shown in Table 3. It is shown in Table 3 that when the machine operates in mode II due to fault in the excitation system, a 10.13% decrease in the output torque is observed.

VII. CONCLUSION

The paper presented the results of a wound field synchronous machine (WFSM) in two modes. Mode I was conventional WFSM, whereas, the machine under loss of excitation (LOE) fault was analyzed in mode II. The LOE fault was avoided by using a stator coil switching technique, where machine was operated as a brushless excited WFSM. A decoupling analysis was conducted and verified between the additional rotor harmonic winding and stator winding. The finite-element analysis was conducted on a 1-kW machine. The FEA results were validated by experiments on a prototype. The percentage decrease in the output torque of the proposed fault tolerant WFSM is 8.23% compare to a conventional WFSM due to accommodation of rotor harmonic turns in the rotor slot. In this work, off-line coil switching technique was performed, in future a more interactive on-line coil switching technique could be analyzed for a twofold advantage i.e., fault tolerant operation, and extended constant power speed range operation.

ACKNOWLEDGMENT

This work was supported by the Korea Institute of Energy Technology Evaluation and Planning (KETEP) and the Ministry of Trade, Industry & Energy(MOTIE) of the Republic of Korea (No. 20174030201780), and in part by the BK21PLUS Program through the National Research Foundation of Korea within the Ministry of Education.

REFERENCES

[1] W. Chai, W. Zhao, and B.-I. Kwon, "Optimal design of wound field synchronous reluctance machines to improve torque by increasing the saliency ratio," *IEEE Trans. Magn.*, vol. 53, no. 11, pp. 1–4, Nov. 2017, Art no. 8206604.

[2] W. Q. Chu, Z. Q. Zhu, J. Zhang, X. Liu, D. A. Stone, and M. P. Foster, "Investigation on operational envelops and efficiency maps of electrically excited machines for electrical vehicle applications," *IEEE Trans. Magn.*, vol. 51, no. 4, Apr. 2015, Art no. 8103510. doi: 10.1109/TMAG.2014.2359008.

[3] C. Rossi, D. Casadei, A. Pilati, and M. Marano, "Wound rotor salient pole synchronous machine drive for electric traction," in *Proc. IEEE Ind. Appl. Conf. 41st IAS Annu. Meeting*, Tampa, FL, USA, Oct. 2006, pp. 1235–1241. doi: 10.1109/IAS.2006.256689.

[4] W. Q. Chu, Z. Q. Zhu, J. Zhang, X. Ge, X. Liu, D. Stone, and M. Foster, "Comparison of electrically excited and interior permanent magnet machines for hybrid electric vehicle application," in *Proc. 17th Int. Conf. Elect. Mach. Syst. (ICEMS)*, Oct. 2014, pp. 401–407. doi: 10.1109/ICEMS.2014.7013504.

[5] T. A. Lipo and Z. S. Du, "Synchronous motor drives-a forgotten option," in *Proc. Intl Aegean Conf. Elect. Mach. Power Electron. (ACEMP), Intl Conf. Optim. Elect., Electron. Equip. (OPTIM), Intl Symp. Adv. Electromech. Motion Syst. (ELECTROMOTION)*, Sep. 2015, pp. 1–5. doi: 10.1109/OPTIM.2015.7426740.

[6] C. R. S. Pierre, "Loss-of-excitation protection for synchronous generators on isolated systems," *IEEE Trans. Ind. Appl.*, vols. IA-21, no. 1, pp. 81–98, Jan. 1985.

[7] B. Mahamedi, J. G. Zhu, and S. M. Hashemi, "A setting-free approach to detecting loss of excitation in synchronous generators," *IEEE Trans. Power Del.*, vol. 31, no. 5, pp. 2270–2278, Oct. 2016.

[8] A. Ghorbani, S. Soleymani, and B. Mozafari, "A PMU-based LOE protection of synchronous generator in the presence of GIPFC," *IEEE Trans. Power Del.*, vol. 31, no. 2, pp. 551–558, Apr. 2016.

[9] M. Ayub, G. Jawad, and B.-I. Kwon, "Consequent-pole hybrid excitation brushless wound field synchronous machine with fractional slot concentrated winding," *IEEE Trans. Magn.*, to be published. doi: 10.1109/TMAG.2018.2890509.

[10] K. Inoue, H. Yamashita, E. Nakamae, and T. Fujikawa, "A brushless self-exciting three-phase synchronous generator utilizing the 5th-space harmonic component of magneto motive force through armature currents," *IEEE Trans. Energy Convers.*, vol. 7, no. 3, pp. 517–524, Sep. 1992. doi: 10.1109/60.148574.

[11] G. Jawad, Q. Ali, T. A. Lipo, and B. I. Kwon, "Novel brushless wound rotor synchronous machine with zero-sequence third-harmonic field excitation," *IEEE Trans. Magn.*, vol. 52, no. 7, pp. 1–4, Jul. 2016.

[12] F. Yao, Q. An, X. Gao, L. Sun, and T. A. Lipo, "Principle of operation and performance of a synchronous machine employing a new harmonic excitation scheme," *IEEE Trans. Ind. Appl.*, vol. 51, no. 5, pp. 3890–3898, Sep./Oct. 2015.

[13] F. Yao, Q. An, L. Sun, and T. A. Lipo, "Performance investigation of a brushless synchronous machine with additional harmonic field windings," *IEEE Trans. Ind. Electron.*, vol. 63, no. 11, pp. 6756–6766, Nov. 2016. doi: 10.1109/TIE.2016.2581759.

[14] Q. Ali, T. A. Lipo, and B. I. Kwon, "Design and analysis of a novel brushless wound rotor synchronous machine," *IEEE Trans. Magn.*, vol. 51, no. 11, Nov. 2015, Art no. 8109804.

[15] Q. Ali, S. Atiq, T. A. Lipo, and B. I. Kwon, "PM assisted, brushless wound rotor synchronous machine," *J. Magn.*, vol. 21, no. 3, pp. 399–404, Nov. 2016.
[16] A. Hussain and B.-I. Kwon, "A new brushless wound rotor synchronous machine using a special stator winding arrangement," *Elect. Eng.*, vol. 100, no. 3, pp. 1797–1804, Sep. 2017. doi: 10.1007/s00202-017-0662-8.
[17] A. Hussain, S. Atiq, and B.-I. Kwon, "Consequent-pole hybrid brushless wound-rotor synchronous machine," *IEEE Trans. Magn.*, vol. 54, no. 11, Nov. 2018, Art no. 8206205.
[18] M. Ayub, A. Hussain, G. Jawad, and B.-I. Kwon, "Brushless operation of a wound-field synchronous machine using a novel winding scheme," *IEEE Trans. Magn.*, vol. 55, no. 6, Jun. 2019, Art. no. 8201104. doi: 10.1109/TMAG.2019.2893883.
[19] M. Ayub, S. S. H. Bukhari, and G. Jawad, "Brushless wound field synchronous machine with third-harmonic field excitation using a single inverter," in *Electrical Engineering*. 2019. doi: 10.1007/s00202-019-00763-3.
[20] A. Hussain, M. Ayub, T. Yazdan, and B. Kwon, "Dual mode dual stator wound rotor synchronous machine for variable speed applications," in *Proc. IEEE Int. Magn. Conf. (INTERMAG)*, Singapore, Apr. 2018, p. 1. doi: 10.1109/INTMAG.2018.8508493.
[21] C. Chakraborty and Y. T. Rao, "Performance of brushless induction excited synchronous generator," *IEEE J. Emerg. Sel. Topics Power Electron.*, to be published. doi: 10.1109/JESTPE.2018.2881068.
[22] J. G. Vaidya, M. L. Bansal, and H. Mansir, "Multiple output decoupled synchronous generator and electrical system employing same," U.S. Patent 5 764 036, Jun. 9, 1998.
[23] C. Chakraborty, S. Basak, and T. R. Yalla, "Synchronous generator with embedded brushless synchronous exciter," *IEEE Trans. Energy Convers.*, to be published. doi: 10.1109/TEC.2019.2900341.

MUHAMMAD AYUB was born in Quetta, Pakistan. He received the B.S. degree from the Balochistan University of Information Technology, Engineering and Management Sciences (BUITEMS), Quetta. He is currently pursuing the Ph.D. degree with the Department of Electrical and Electronic Engineering, Hanyang University, Ansan, South Korea. He was a Lecturer with BUITEMS. His research interest includes electric machine design and control.

SHAHID ATIQ was born in Punjab, Pakistan. He received the bachelor's and master's degrees from the University of Engineering and Technology Taxila, Pakistan, and the Ph.D. degree from Energy Conversion Systems Laboratory, Hanyang University, South Korea. He held different managerial and educational posts at various institutions. He is currently serving as an Associate Professor and the Head of the Department of Electrical Engineering, Khwaja Fareed University of Engineering and Information Technology, Rahim Yar Khan, Pakistan.

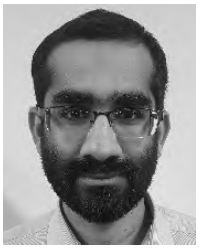

GHULAM JAWAD SIREWAL was born in Tando Allahyar, Pakistan, in 1988. He received the B.E. degree in electrical engineering, in 2011, and the Post Graduate Diploma degree in electrical power engineering from the Mehran University of Engineering and Technology, Jamshoro, Pakistan. He is currently pursuing the Ph.D. degree with the Department of Electrical and Electronic Engineering, Hanyang University, Ansan, South Korea. His research interest includes electric machine design and control.

BYUNG-IL KWON was born in 1956. He received the B.S. and M.S. degrees in electrical engineering from Hanyang University, Ansan, South Korea, in 1981 and 1983, respectively, and the Ph.D. degree in electrical engineering and machine analysis from the University of Tokyo, Tokyo, Japan, in 1989. From 1989 to 2000, he was a Visiting Researcher with the Faculty of Science and Engineering Laboratory, University of Waseda, Tokyo, Japan. In 1990, he was a Researcher with the Toshiba System Laboratory, Yokohama, Japan. In 1991, he was a Senior Researcher with the Institute of Machinery and Materials Magnetic Train Business, Daejeon, South Korea. From 2001 to 2008, he was a Visiting Professor with the University of Wisconsin–Madison, Madison, WI, USA. He is currently a Professor with Hanyang University. His research interest includes the design and the control of electric machines.